# Lime Cake as an Alternative Stabiliser for Loose Clayey Loams

Assadi-Langroudi, A.[1,*], Ghadr, S.[2], Theron, E[3], Oderinde, S.A.[4], Katsipatakis, E.M.[4]

[1,*] Senior Lecturer, University of East London, London
E16 2RD, England [* Corresponding Author]
E. A.AssadiLangroudi@uel.ac.uk
T. +44(0) 20 8223 2170

[2] University of Urmia, Iran

[3] Central University of Technology Free States, South Africa

[4] University of East London, London, England

**Abstract:** Lime Cake (Precipitated Calcium Carbonate PCC), a bi-product of sugar production, is proposed as a stabiliser for improvement of loose silty clayey loams. Two inorganic pedogenic and organic precipitated calcium carbonate polymorphs are artificially synthesized into a base loosely compacted loamy soil. Formation, micromorphology, quality of cementing bonds, and physiochemical interactions in the interlayer are modelled at molecular level and verified by a suite of micro-analytical spectrometry techniques. Emphasis is put into determining the impacts of polysaccharides on soil strength and implications on soil pore anatomy. Erodibility, compressibility, volumetric change, and hydro-mechanical behaviour of base, and modified soils at yield and post-yield states are studied. Anomalies in suction-controlled post-yield stress-strain behaviour of modified soils are discussed and explained within the tenets of mechanics of composite soils with double porosity.

PCC-reinforcement offers the closest possible packing at optimum water content. Desiccation cracking remains likely, but at relatively higher lower-bound water contents. Under low confinement levels and unsaturated state, strain-hardening prevails. Loss of shear strength on saturation is minimal. When saturated, PCC-reinforced soil develops substantially high levels of shear strength at all strain levels. Higher levels of confinement are needed for organic fibrous and onion-skin coating

matters to effectively encrust the soil pore network; such high levels however leads to formation of an unwelcomed brittle, strain-softening stress-stress behaviour.

Keywords: Precipitated Calcium Carbonate, fibres, organic, soil, stabilisation, unsaturated, double porosity

## 1. Introduction

There is a global drive towards development and deployment of natural inspired technologies and materials in ground improvement practice to relax the strain on quarries and to establish the broadly neglected symbiosis between grounds' natural and enhanced engineering functions. Common cementitious stabilisers are reviewed by Chen [1] and Houston et al. [2] and include lime, cement, fly ash, kiln dust, potassium and ammonium compounds, silicates and polymers [3-4]. In addition to traditional stabilisers, the use of wastes and recycled materials have received much interest, over the past few years as alternatives to common cementitious stabilisers, among which organic fibres have relatively received relatively little attention. This paper outlines scopes for using Lime Cake Precipitated Calcium Carbonate (PCC) with organic fibres as alternative to natural calcium carbonate for improvement of loose loamy soils.

Loamy soils present a range of interconnected problematic ground conditions with often catastrophic implications including debris flow in hillslopes and instability in shoulders of aged embankments. Use of lime piles in distressed loamy hillslopes and embankments is a well-established remedial measure for improving soils' bearing capacity and stiffness, and also to rectify problematic volumetric behaviours. The procedure involves in introduction of calcium oxide to soil and formation of calcium hydroxide following an exothermic interaction between calcium oxide and soil water. Soil's clay component rapidly flocculates, leading to formation of a modified and friable microstructure. Calcium-enriched electrolytes seep into clay matrix and trigger a suite of ion exchange events [5-6], that are mainly associated with pH-dependent charges at the edges of clay platelets. $Ca^{2+}$ ions exchange with monovalent $Na^{+}$ ions at clay stern layer, soil solution pH increases, leading to alterations in pH-

dependent positive charges. Deprotonation of clay [7] leads to liberation of hydroxides, further increase in pH, and formation of calcium silicate hydrate (C-S-H) and calcium aluminate hydrate (C-A-H) gels at quartz (i.e. sand and silt) contact points. This process is broadly known as pozzolanic reaction and is believed to substantially improve soil's shear strength. Comprehensive reviews of mechanisms of clay-lime reaction and technologies of soil lime stabilisation include the seminal works of [8-10]. The pozzolanic reactions need a source of silica or alumina (deprotonated clay) as well as a source of calcium ions. In absence of calcium oxide, the required $Ca^{2+}$ can alternatively be supplied by readily-soluble carbonates in soil, or calcitic substances including highly basic construction wastes (i.e. rubble including crushed concrete, plaster and stucco) comprising $Ca^{2+}$/$Mg^{2+}$ silicates and hydroxides [11]. This paper examines the scopes for using a peculiar type of Precipitated Calcium Carbonate (PCC) from food production industry (known as Lime Cake) to function as the $Ca^{2+}$ source required for formation of C-S-H gels in loamy soils.

Synthetic or Precipitated Calcium Carbonate (PCC) is a by-product from a diverse range of production industries and has found application in treatment and remediation of wastewater, as cementitious blends [12], as filler and coating pigment in paper industry [13], as nano-sized filler for PVC plastisols and coatings in car industry [14], in powdered beverage mix containing rapidly dissolving calcium [15], and in biomedical discipline as a component of anchor tissue engineered cartilage used in treatment of defected joints [16]. PCC in form of Lime Cake is a non-toxic product of sucrose ($C_{12}H_{22}O_{11}$) juice purification during sugar production (Equations 1 to 2).

$$C_{12}H_{22}O_{11}(aq) + Ca(OH)_2 \rightarrow C_{12}H_{22}O_{11}.CaO\ (aq) \quad [1]$$

$$C_{12}H_{22}O_{11}.CaO\ (aq) + CO_2\ (g) \rightarrow CaCO_3\ (s) + C_{12}H_{22}O_{11}\ (aq) \quad [2]$$

Since the early 1840s in the UK and the late 1930s in the United States, PCC has been manufactured as bi-product from sugar purification. Today, over 120 countries produce a total of >120 $MT.a^{-1}$ sugar, 30% of which is produced using sugar beet [17]. The PCC waste production from sugar refining marked a high rate of over 0.1 $MT.a^{-1}$ in 2008 [18]. A proportion of the global PCC waste is used in pharmaceutical,

agriculture and food packaging industry. A larger proportion, however, is stockpiled on site or landfilled. This amounted to 80 kT in 2016, at about 10 $kT.a^{-1}$ rate for every 100 $kT.a^{-1}$ of refined sugar beet in Khorezm Sugar Company in Uzbekistan and 379 $KT.a^{-1}$ for every 1.3 $MT.a^{-1}$ of refined sugar beet in British Sugar Company across its six manufacturing sits [17]. Potential use of PCC in earthworks can significantly ease the pressure on landfills. PCC includes calcium carbonate (60-85%), organic matters (10-15%), and trace levels (<1%) of nitrogen, phosphorus and potassium [17]. Organic matters include pectin, a complex set of polysaccharides and albumen. Limestone is heated to >1000°C in a lime kiln to release $CO_2$(g) and Calcium Oxide, which is then added to sugarbeets juice in combination with $CO_2$ to re-precipitate a peculiar polymorph of calcium carbonate that contains non-sucrose cytoplasmic constituents of sugar beet root cells in colloidal form. Calcium carbonate is then filtered out of purified diffusion juice [19].

The scopes for the use of precipitated calcium carbonate in improving loose clayey loams have received some recent interest [20-21], yet, little is known on the role of organic matters which are abundant in PCC Lime Cake, and specifically the implications on carbonate precipitation, physiochemical interactions in the clay interlayer, and formation of C-S-H gels. We argue that whilst organic component of PCC can further enhance the stability of soil aggregates, their water retention capacity and hydraulic conductivity, consequent modification to micro-structure generates strain-softening at certain confinement levels.

## 2. Materials and Methods

### 2.1 Rationale

Implications of using PCC Lime Cake as an alternative to lime in chemical stabilisation of loose silty clayey loams are studied via an experimental programme on artificial soils. Whilst the binding role of calcium carbonate - from Lime Cake - in clayey loams is universally appreciated, very little is known of the effect of organic constituents of Lime Cake on yield and post-yield behaviour of treated loam. To

this end, two soil mixtures comprising 65% by-weight natural loam adjusted with kaolinite clay and mixed with two strains of calcium carbonate, PCC Lime Cake and pedogenic of similar content.

Saturated lime-stabilised soils generally enjoy higher strength and stiffness; their brittle and contractive response to excessive loading [22] however continues to be a challenge. Assadi-Langroudi and Jefferson [21] recently reported a critical composition of 10 to 20% clay content and 20 to 25% calcium carbonate at which the problematic behaviour is amplified. To ensure this problematic behaviour is taken into account in development of new geo-composites, natural loam was mixed with 15% by weight of kaolinite clay to bring the calcium carbonate content to the potentially problematic 20% level. In addition to two organic and inorganic calcareous specimens, a third reference non-calcareous specimens were designed and synthesised to ascertain the cementing role of calcium carbonate and stress-strain implications.

## 2.2 Materials and Test Specimens

Natural firm brown sandy clayey silt (i.e. loam), adjusted with kaolinite clay and mixed with pedogenic calcium carbonate and PCC Lime Cake were adopted as testing materials. The natural silt was obtained from a 0.7m deep exploratory open trench from Roding Valley Essex (TQ420 923). The natural silt is known to be very soft to very stiff, highly compressive with the risk of severe differential settlements at slow rate dependent on shear strength and consolidation characteristics. The PCC Lime Cake was supplied in kind by Thames Refinery located in Royal Docklands in East London. The kaolinite clay used was a commercial grade (i.e. PolWhite–E English China refined clay, $D_{50}$=75 μm, $C_u$=9.1, $C_g$=19.3). The extra pure pedogenic Calcium Carbonate powder (8-9 pH, <2000 ppm $Na^{+}$, <2000 ppm $Mg^{3+}$, <200 ppm $Fe^{3+}$, <1000 ppm $Si^{+4}$) was supplied by Fishers Scientific. Three composite geomaterials (A, B and C) were prepared by mixing predetermined dry masses of natural silt, Kaolinite clay, pedogenic Calcium Carbonate and PCC Lime Cake. To analyse the role of organic matters in the precipitation process, infra-red (IR) spectra (transmittance) were generated for testing specimens, using a Bruker Vertex 70 apparatus. Thin pellets of powdered samples were obtained from test specimens were obtained from

test specimens at 0° and 90° to the shearing axis and spectra of the crystals were scanned within 400-4000 $cm^{-1}$ absorption band range. X-ray diffractometry (XRD) was undertaken on a subset of specimens to ascertain the particle-level interactions and implications on soil's mineralogical composition. The Bragg's law was used to interpret the XRD data (CuKα radiation, λ=1.5406 A°, V=40 kV, n=1, scanning from $2\theta = 3° \; to \; 90°$ at step time 3s). Physical and index properties of the three composites were determined in compliance with the British Standard and are summarized in Table 1. Particle size distribution curves obtained by a combination of sieving analysis and pipette experiments are plotted in Fig. 1: Specimen A is bimodal (pronounced mode sizes on 12.25 μm and 102.5 μm) poorly sorted (skewness sk=-0.012 μm) very fine sandy medium silt soil. Specimen B is trimodal (pronounced modes on 12.25 μm, 102.5 μm, and 40 μm) very poorly sorted (skewness sk=-0.023 μm) very fine sandy medium silt soil (mean size $\bar{x}$=17.67 μm, sorting $\sigma$=4.205 μm). Specimen C is polymodal (pronounced modes on 12.25 μm, 30 μm, and 102.5 μm) very poorly sorted (skewness sk=-0.249 μm) very fine sandy medium silt soil (mean size $\bar{x}$=19.24 μm, sorting $\sigma$=6.896 μm).

Shear box test specimens (A, B, and C - Table 1) were remoulded using static compression via a uniaxial compression loading frame; soil was compressed (in a single lift) to the intended unit weight on the dry-of-optimum side and into 60 mm x 60 mm x 20 mm standard size shear box mould. The compression effort used was adjusted and retained at 0.5 mm/min rate. Placement water content was retained at a constant 17-18% range, offering a $w/w_{opt}$ of 0.7 to 0.9. For each soil combination, six identical specimens were remoulded to allow studying the stress-strain relationship under both saturated and unsaturated conditions. The full account of the testing campaign is discussed in subsequent sections. Filter paper method was employed to determine the Soil Water Characteristic parameters. The van Genuchten (vGM) and Fredlund and Xing FX [23-24] models were deployed to plot the Soil Water Characteristic Curve (SWCC). Figure 2 and Table 2 present the SWCC and water retention properties of testing specimens. The findings will be discussed in depths in the subsequent sections.

## 2.3 Immediate Observations

Presence of pedogenic calcium carbonate appears to have caused a decrease in liquid limit (specimens A and B compared); whilst organic matters in PCC give a substantial rise to the liquid limit (specimens C and B compared). This may imply a relatively greater resilience of PCC-reinforced soils towards erosion. Desiccation cracking in PCC-reinforced soils are likely but at a relatively higher lower-bound water contents; this marks an advantage of using PCC Lime Cake in groundworks in predominantly hot and arid climates. Maximum dry density in calcareous specimens appears to be marginally greater than that in non-calcareous specimens. The relatively closer packing in specimen B as compared with A (i.e. lower void ratio) can be attributed to the diminished potential of clay platelets to swell. PCC significantly adds to the water absorption/retention capacity of the soil. Secondary electron micrographs of specimen C also suggest that a resin-like matrix covers the pore network, leading to the formation of the closest packing among all specimens compacted at the optimum water content (Fig. 3). Both residual water content and air entry value increase in presence of calcium carbonate compounds. This increase in remarkably higher in presence of PCC as compared with Pedogenic carbonates, possibly due to their organic contents. Greater residual water content allows greater water storage capacity in soils, thereby delayed surficial waterlogging in the event of heavy precipitation. The greater AEV measured in specimen C suggests the transformation of clay connectors (in loamy base soil) into almost airtight units upon interacting with the PCC. This is evident from the microscopy micrograph in Fig. 3. Interactions are further discussed at molecular level.

## 2.4 Physiochemical Interactions at Interlayer

Vibrational spectroscopy is used to gain an insight into hydration characteristics, interlayer cations and bonding qualities in specimens B and C (i.e. modified with natural and PCC Lime Cake precipitated carbonates). The technique specifically allows tracking alterations in the Si-O vibrations resulting from changes in crystal symmetry. Presence of pectin was deemed likely to cause such alterations.

Absorbance spectra were obtained for specimens B and C at hygroscopic water content. Samples were taken ahead of shearing, in an undisturbed state and at 0° and 90° angle to the shearing axis. IR spectra was recorded and presented in Fig. 4a-b. IR spectra of specimen B and C show a strong absorption peak at $\lambda$ = 795 $cm^{-1}$, which corresponds to calcite. Footprints of other stable polymorphs of calcium carbonates are visible in IR band peaks at 1427 $cm^{-1}$ and 875 $cm^{-1}$. The strong absorption peak at 752.4 $cm^{-1}$ in specimen B represents younger polymorphs of calcium carbonate). Peak on 3620 $cm^{-1}$ represents exposed hydroxyl groups and is an indication of clay deprotonation into pozzolan. For specimen C, the higher absorbance at 1650 $cm^{-1}$ than 1750 $cm^{-1}$ is a characteristic of a high methoxyl pectin.

Figure 4c presents the XRD spectrograph for specimen B. It is pertinent to emphasis here that XRD spectra is purely qualitative and does not show the amount of minerals present since the signal intensity in form of peaks and depressions are controlled by both mineral orientation and population. Bragg's equation was used to determine the d-spacing of atomic planes from scanning angle $2\theta$ and input wavelength. Peaks at $2\theta$ angles 73.5, 62.5, 60.0, 55.0, correspond to Na-carbonates. The Na-primary minerals are abundant in the natural clayey silt component and are probably stemmed from weathering of alumina-silicate minerals through carbonation into solutions of carbonates and bi-carbonates of sodium, with footprints of sodium carbonate on Fig. 4c in form of peaks at $2\theta = 60.8°$ and $76°$. Na-minerals interact with water to form a broad range of H-silicates and amorphous silica precipitates. In Fig. 5, interaction of Na-primary minerals and water releases H-silicates and a range of cation-hydroxides, leading to an increase in the pH at soil solution phase (see Table 1). As pH exceeds the point of zero net charge (PZNC), hydroxyl tails of clay begin to donate protons (Fig. 6a). The liberation of $H^+$ allows the deprotonated oxygen atoms to absorb free $Na^+$ cations, forming Sodium Aluminium Silicate hydrate zeolites ($NaAlSiO_4.H_2O$). This has clearly appeared in the $2\theta \sim 21°$peak on the XRD spectra in Fig. 4c. The silicon of H-silicates shares an electron with clay's deprotonated oxygen atoms to form Al-O-Si-O bonds (Fig. 6b). This balances the pH to nearly neutral levels. Divalent $Ca^{2+}$ ions from PCC replace the $Na^+$ on tetrahedral unit, benefitting from its higher cation exchange capacity. In Fig. 7, Calcium ion

sits in between clay and pectin. The footprints of this peculiar form (which is unique to specimen C) appears in Fig. 4a-b in the difference in intensity of the IR bands at 875 $cm^{-1}$ and 3640 $cm^{-1}$ between specimen B and C. The bands at 875 $cm^{-1}$ and 3640 $cm^{-1}$ are associated with stretching vibrations of Ca-OH. Such substitution induces an excess positive charge, allowing the absorption of -$CO_3^{2-}$ anions. Calcium carbonate nucleates on clay surface. The released $Na^+$ ions react with the free $Cl^-$ anions to form sodium chloride precipitates, coating the silica-indurate calcareous clayey connectors. The O-Si-O bonds assist hydrogen bonds within the clay intra-lattice space.

Ligand exchange between the hydroxyl tail of clay and negatively charged pectin balances the net negative charge upon formation of chains of anions, cations, and neighbouring clay platelets (Fig. 7). Significant changes in the silicate (Si-O) stretching region (1150 to 950 $cm^{-1}$) is evident in Fig. 4a-b between specimen B and specimen C: peaks in these regions gain greater intensity in specimen C as compared with specimen B. This can be attributed to disturbance to soil microfabric, probably following the ligand exchange. The 20% transmittance difference between band intensity at 1078 $cm^{-1}$ and 1086 $cm^{-1}$ between specimens B and C reflect on the altered water retention and plasticity of complex chains of deprotonated clay – pectin – cation – pectin formed upon ligand exchange. The observed elevated levels of plasticity in specimen C is attributed to the existence of such chains and the reduced intra-lattice pore volumes (Fig. 3). The relative higher air-entry value obtained is specimen C is consistent with this argument: relatively closer packing of clay domain upon ligand exchange renders smaller pore radii and enhances the air entry value (see similar case reported in [25]). The organic hydrophilic component of chains explains the greater orders of shrinkage limit in specimen C.

The major mid-IR bands for C-S-H gels typically appear at 970 $cm^{-1}$ (associated with the Si-O stretching vibrations), 660-670 $cm^{-1}$ (associated with the Si-O-Si bending vibration) and 450-500 $cm^{-1}$ (associated with the deformation of $SiO_4$ tetrahedra). Theoretically, the ligand exchange interferes with the pozzolanic reactions and as such is expected to affect the frequency and/or intensity of these bands. In Fig. 4, the IR band for specimen B peaks at 660-670 $cm^{-1}$ and 465 $cm^{-1}$. Mid-IR bands peak for specimen

C is limited to 469 $cm^{-1}$ only. Any decrease in the wavenumber within the mid-IR band range indicates the de-polymerization of the silicate chains. The shift of Si-O stretching band position toward lower wavenumber values in specimen C confirms that ligand exchange has influenced the composition of C-S-H gel during the hydration process.

## 2.5 Hydro-Mechanical Testing Methods

Eighteen drained saturated and unsaturated direct shear tests were conducted to determine the effective shear strength parameters at peak (P), critical state (C), and residual strains (R). Specimens were sheared at 140kPa, 280kPa, and 420kPa normal stress at slow rate of 0.305 $mm.s^{-1}$. The adopted dry-of-optimum placement condition and low initial void ratio (i.e. dense packing) led to marginal levels of dry contraction in unsaturated specimens upon $K_0$-loading. This combined with the generally dilative shear response of unsaturated specimens allowed shearing along a constant water content path. Particle size distribution (PSD) data (derived from the Pipette test) was fitted using the Levenberg-Marquardt algorithm. For unsaturated specimens, PSD data was plugged into Arya-Paris Pedo-Transfer Function [26-28] to build a suite volumetric water content - suction curves, for a wide range of void ratio (that corresponds with the experimentally measured shear strains). Matric suction was determined for varying shear and packing states, at constant water content. The PTF models were scaled using the advanced Logistic Growth method for silty loams [29], for strictly controlled ambient conditions (T=20°C, $\mu_a$=1.8E-5 $N.s.m^{-2}$, $\mu_w$=1.0E-3 $N.s.m^{-2}$, $T_s$=72.75 $mN.m^{-1}$). Matric suction values were paired with shear strain for unsaturated test specimens.

# 3. Suction-informed Shear Strength

## 3.1 Stress-Strain behaviour

Figure 8 illustrates the suction-stress-strain envelopes. As one would expect, all soil specimens developed greater levels of shear strength under unsaturated conditions for all strain levels (P, C, R).

Calcite cementation for partially saturated soils (specimen B) increased the yield stress (P) and brittleness; cementation generated a clear strain-hardening plastic behaviour. Here, the volume contraction stemmed from $k_0$-loading decreased by 5%. The normal stress (and hence confinement level) appears to have a control on the yield shear stress level, but no notable effect on post-peak plastic behaviour.

The strain-hardening is influenced by the structure-based behaviour of soil with double porosity (common in cemented soils). Assadi-Langroudi and Jefferson [30] recently proposed a new form of effective stress principle that explains the dilative (Fig. 9) and strain-hardening plastic response in unsaturated cemented soils. Discussing this soil model falls beyond the scopes of present work and interested readers are referred to [31-32] for in-depth discussion.

Dilative, strain-hardening plastic response prevailed in calcareous specimens (Fig. 8b,e,h and Fig. 9b,e,h). During shearing, the simultaneous decrease in matrix suction and increase in post-peak shear stress marked a new trend that contests the broadly accepted relevance of capillary forces and suction-hardening [33]. This discrepancy is here conceptually discussed at micro-level: Presence of calcites in loam allows $Ca^{2+}$ divalent cations to replace clay monovalent $Na^{+}$ cations, facilitating the mutual coherence between clay platelets: The cation cloud contracts, leading to an increase in Van der Waals attractive forces; attractive forces continue to increase beyond repulsive forces to trigger rapid coagulation in clay platelets. Coagulation has two key effects: First, coagulation enhances the resistance of soil against wetted erosion and structural modification. This is consistent with the observed greater friction angle in cemented specimen B as the sharp asperities of quartz particles (i.e. β) benefit from enhanced coordination number that is supplied by clay connector/coat units during shearing. Secondly, the porous medium begins to exhibit two scales of porosity upon coagulation: A new domain of micropores appear in aggregates and macropores appear in between aggregates. Initially, excess negative pore water pressure forms at the micro-pores phase, leading to the formation of a pore water pressure gradient between micro- and macro-pores. Pore water begins to flow into micro-pores to

balance the pressure gradient. Intra-lattice spaces in clay platelets begin to adsorb water and expand. Two interrelated principles are recalled: matric suction is fundamentally controlled by micro-pores at clay aggregate level and swelling is followed by a decrease in matric suction. The strain-hardening seen in unsaturated calcareous soils with pedogenic carbonates is hence probably not suction-induced. This lends evidence to the significance of chemical cementation in mechanical properties of unsaturated soils.

Yield stress (P) in PCC-reinforced unsaturated specimens at 140 and 280 kPa net stress was reached at slightly lower orders than in non-calcareous and calcareous specimens. This is consistent with the strain-softening seen in PCC-reinforced soils and agrees with typical behaviour of soils with high organic contents. Maximum yield stress (P) was achieved in specimen C at the high 420 kPa net stress. This is an interesting finding: Higher levels of confinement is needed for organic fibrous matters (and onion-skin coatings) to effectively encrust the soil pore network. This may stand as a technical limitation in use of PCC for ground improvement. Double porosity and the emerging forms of soil models for cemented soils with double porosity continue to be valid for PCC reinforced specimens, but these models are constrained to loose soils and low confinement levels only. Common forms of principle of effective stress should be deployed when studying the behaviour of PCC-reinforced soils at high confinement: Upon yielding and irrespective of normal stress levels (i.e. here an indication of confinement level), PPC-reinforced unsaturated specimens exhibited a clear brittle behaviour followed by strain-softening. Yield appears to be almost simultaneous with a drop in matric suction at low normal stresses and increase in matric suction at high normal stress levels. The strain softening is probably manipulated by PCC's organic matters. Stemmed from the PTF models and for low confinement levels, the packing state transition - upon shearing - led to the formation of two different levels of pore spaces with possible control on soil matric suction: At small strains, the 0.231-0.257 µm pores (associated with 9-20 µm particles in PTF model) controlled the matric suction. At large strains and following modification of the packing state, the wider range 0.231-1.131 µm pore size (associated with 10-30 µm

particles in PTF model) controlled the matric suction. This double porosity quality of packing highlights the control of structure on matric suction.

### 3.2 Strength

Generally, unsaturated specimens developed brittle behaviour and elevated levels of yield shear stress as compared with their saturated identical counterparts.

For both saturated and unsaturated specimens, effective friction angle gained higher values in cemented specimen B as compared with specimen A; the increase appears to be more pronounced under fully saturated conditions. The relatively more pronounced increase in friction angle in saturated specimens can be attributed to the greater levels of wetted-induced 'contact modification' in loam and in absence of carbonate shields: Calcite units coat and interact with clayey inter-particle connectors to generate a suite of C-S-H nodules within the aluminosilicate structure. Unreinforced connectors fail to fully protect the quartz particles against 'edge-chipping', thereby gaining only a slim rise in friction angle. The shear strength loss upon saturation amounts to 60-65% in non-calcareous specimens, 45-60% in calcareous specimens, and 20-45% in PCC-reinforced specimens. Saturated PCC-reinforced soil developed the greatest shear strength values at ultimate, critical and residual states. This ties in with the earlier discussion on clay-carbonate-fibres interaction.

## 4. Conclusions

Implications of using PCC Lime Cake as an alternative to lime in chemical stabilisation of loose silty clayey loams are studied. Observations suggest that:

1. Calcite in loam adds to the unsaturated yield stress and brittleness and forms a strain-hardening dilative plastic behaviour that is not suction-induced but controlled by the structure.
2. Upon modification, strain-hardening disappears under moderate to high confinement levels.

3. Modification leads to formation of complex chains of deprotonated clay – pectin – cations – pectin, de-polymerization of silicate chains, and alteration of C-S-H gels composition.
4. Modification transforms loose loams into a peculiar geo-composite, adaptable to extreme climates through an increase in plasticity and decrease in intra-lattice pore volumes.
5. Modification leads to an increase in shrinkage limit, compressibility at optimum water content, residual water content, water storage capacity, and air entry value.
6. Saturated modified soils develop high levels of shear strength at ultimate, critical and residual states. The loss of shear strength on saturation amounts to 60-65% in non-calcareous loams, 45-60% in calcareous loams, and 20-45% in PCC modified loams.

## 5. References


1. Chen FH (1988) Foundations on Expansive Soils, 2nd Edition, Elsevier Scientific Publishing, Amsterdam, The Netherlands.

2. Houston SL, Dye HB, Zapata CE, Walsh KD and Houston WN (2011) Study of expansive soils and residential foundations on expansive soils in Arizona. Journal of Performance of Constructed Facilities 25(1):31–44.

3. Petry TM and Little DN (2002) Review of stabilization of clays and expansive soils in pavement and lightly loaded structures history, practice and future. Journal of Materials in Civil Engineering 14(6):447–460.

4. Mirzababaei M, Arulrajah A, and Ouston M (2017) Polymers for stabilization of soft clay. Procedia Engineering 189:25-32.

5. Little D (1995) Handbook for Stabilization of Pavement Subgrade and Base Courses with Lime. Lowa: Kendall Hunt.

6. Broms B and Boman P (1977) Lime columns a new type of vertical drain. In: Proceedings of the 9th International Conference of Soil Mechanics and Foundation Engineering, 1:427-432, Tokyo.

7. Van Olphen H (1977) An introduction to clay colloid chemistry, for clay technologists, geologists, and soil scientist. New York, John Wiley & Sons.

8. Bell FG (1989) Lime stabilisation of clay soils. Bulletin of the International Association of Engineering Geology. 39(1):67-74.

9. Rogers CFG, and Glendinning S (1997) Improvement of clay soils in situ using lime piles in the UK. Engineering Geology 47:243-257.

10. Beetham P, Dijkstra T, Dixon N, Fleming P, Hutchison R, and Bateman J (2015) Lime stabilisation for earthworks: a UK perspective. Proceedings of the Institution of Civil Engineers Ground Improvement, 168(GI2):81-95.

11. Norra S, Fjer N, Li F, Chu X, Xie X, and Stuben D (2008) The influence of different land uses on mineralogical and chemical composition and hirozonation of urban soil profiles in Qingdao, China. Journal of Soil and Sediments 8(1):4-16.

12. Santos RM, Georgakopoulos E, Manovic V, and Chiang YW (2016) Producing value-added mineral products from metallurgical slag. Canadian Chemical Engineering Conference. Quebec. Canada.

13. El-Sherbiny S, El-Sheikh SM and Barhoum A (2015) Preparation and Modification of Nano Calcium Carbonate Filler from Waste Marble Dust and Commercial Limestone for Papermaking End Application. Powder Technology 279:290-300.

14. Zhang H, Chen JF, Zhou HK, Wang GQ and Yun J (2002) Preparation of Nano-Sized Precipitated Calcium Carbonate for PVC Plastisol Rheology Modification. Journal of Material Science Letters 21(16):1305-1306.

15. Valencia D and Calapini SA (2004) Powdered Beverage Mix with Rapidly Dissolving Calcium. US Patent 6,833,146

16. Kreklau B, Sittinger M, Mensing MB, Voigt C, Berger G, Burmester GR, Rahmanzadeh R, and Gross U (1999) Tissue Engineering of Biphasic Joint Cartilage Transplants. Biomaterials. 20(18):1743-1749.

17. Shoira M (2006) Application of defecation lime from sugar industry in Uzbekistan. Industrial Ecology Royal Institute of Technology. Stockholm. TRITA-KET-IM 2006:3.

18. Hanks DA, and Shaw D (2008) Precipitated Calcium Carbonate (PCC) from sugar processing by products for use in cementitious applications and methods thereof. United States Patent US2008/0210134 A1.

19. Inkret JM (1996) Effects of precipitated calcium carbonate from sugar purification on crusting soils. Montana State University.

20. Palomino AM, Burns SE, and Santamarina JC (2008) Mixtures of fine-grained minerals – kaolinite and carbonate grains. Clays and Clay Minerals. 56(6):599-611.

21. Assadi-Langroudi A and Jefferson I (2013) Collapsibility in calcareous clayey loess: a factor of stress-hydraulic history. International Journal of GEOMATE. 5(1):620-627.

22. Ismail MA, Joer HA, Sim WH, and Randolph MF (2002) Effect of cement type on shear behavior of cemented calcareous soil. Journal of Geotechnical and Geoenvironmental Engineering. 128(6):520-529.

23. Fredlund DG, and Xing A (1994) Equations for the soil-water characteristic curve. Canadian Geotechnical Journal 31:521-532.

24. Van Genuchten MT (1980) A closed-form equation for predicting the hydraulic conductivity of unsaturated soils. Soil Science Society of America Journal 44:892‑898.

25. Zhang X, Mavroulidov M, and Gunn MJ (2017) A study of the water retention curve of lime-treated London Clay. Acta Geotechnica 12:23-45.

26. Arya LM, Leij F, Van Genuchten MT, Shouse PJ (1999) Scaling parameter to predict the soil water characteristic from particle-size distribution data. Soil Science Society of America Journal (63):210–519.

27. Arya LM, Paris JF (1981) A physicoempirical model to predict the soil moisture characteristic from particle-size distribution and bulk density data. Soil Science Society of America Journal 45:1023–1030.

28. Haverkamp R, Parlange JY (1982) Comments on: a physicoempirical model to predict the soil moisture characteristic from particle-size distribution and bulk density data. Soil Science Society of America Journal 46:1348–1349.

29. Arya LM, Paris JF (1982) Reply to comments on a physicoempirical model to predict the soil moisture characteristic from particle-size distribution and bulk density data. Soil Science Society of America Journal 46:1348–1349.

30. Assadi-Langroudi A, and Jefferson I (2016) The response of reworked aerosols to climate through estimation of inter-particle forces. International Journal of Environmental Science and Technology 13(4):1159-1168.

31. Assadi-Langroudi A, Ng'ambi S, and Smalley I (2018) Loess as a collapsible soil: some basic particle packing aspects. Quaternary International 469(A):20-29.

32. Assadi-Langroudi A (2014). Micromechanics of collapse in Loess. University of Birmingham. England. UK.

33. Bagherieh AR, Khalili N, Habibagahi G, and Ghahramani A (2009) Drying Response and Effective Stress in a Double Porosity Aggregated Soil. Engineering Geology, 105:44-50.

List of Figures 415



431

List of Tables 432



435

436

Table 1

| Specimens | A | B | C |
|---|---|---|---|
| Composition | | | |
| Natural sandy clayey silt | 65% | 65% | 65% |
| Kaolinite | 35% | 15% | 15% |
| Pedogenic Calcium Carbonate | 0% | 20% | 0% |
| PCC Lime Cake | 0% | 0% | 20% |
| Physical properties | | | |
| $w_{opt}$: % | 19.0 | 18.5% | 26.0% |
| $\rho_{d-max}$: kg.m$^{-3}$ | 1561.9 | 1690.0 | 1920 |
| $w_i$:% | 17.0 | 17.0 | 18.0 |
| $\rho_{d,i}$: kg.m$^{-3}$ | 1560.0 | 1670.0 | 1760.0 |
| $e_i$ | 0.73 | 0.56 | 0.42 |
| $w/w_{opt}$ | 0.9 | 0.9 | 0.7 |
| $G_s$ | 2.7 | 2.6 | 2.5 |
| LL:% | 64.0 | 56.0 | 65.0 |
| PL:% | 27.5 | 19.8 | 25.0 |
| PI: % | 36.5 | 36.2 | 40.0 |
| A | 7.5 | 3.3 | 2.7 |
| pH (soil solution) | 6.9 | 8.6 | 8.1 |
| SL:% | 10.2 | 11.0 | 12.8 |
| $D_{50}$: mm | 0.021 | 0.019 | 0.028 |
| Sub 2-µm: % | 4.9 | 11.1 | 15 |

Table 2

| | Fredlund and Xing [23] - FX | | | | | | Van Genuchten [24] - vGM | | | | |
|---|---|---|---|---|---|---|---|---|---|---|---|
| | $a$ | $n$ | $m$ | $h$ | $\theta_r$: % | $AEV$: kPa | $a$ | $n$ | $m$ | $\theta_r$: | $AEV$: kPa |
| A | 1242.5 | 0.485 | 3.32 | 14229 | 7.2 | 16.96 | 7.12e-5 | 0.479 | 4.11 | 10 | 17.56 |
| B | 2499.9 | 0.420 | 3.19 | 39070 | 11.3 | 19.97 | 2.68e-5 | 0.417 | 3.81 | 10 | 20.87 |
| C | 1620.8 | 0.530 | 2.14 | 47582 | 13.6 | 84.10 | 2.76e-5 | 0.494 | 3.48 | 10 | 74.45 |

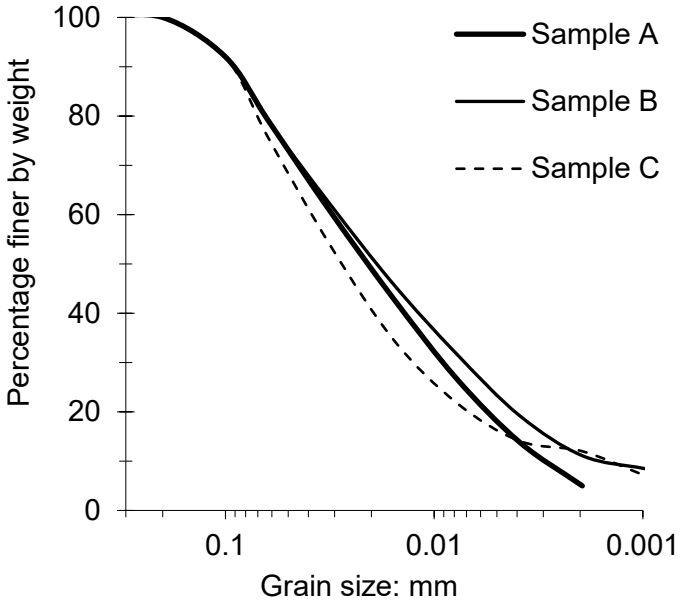
Sample A
Sample B
Sample C
Percentage finer by weight
100
80
60
40
20
0
0.1
0.01
0.001
Grain size: mm

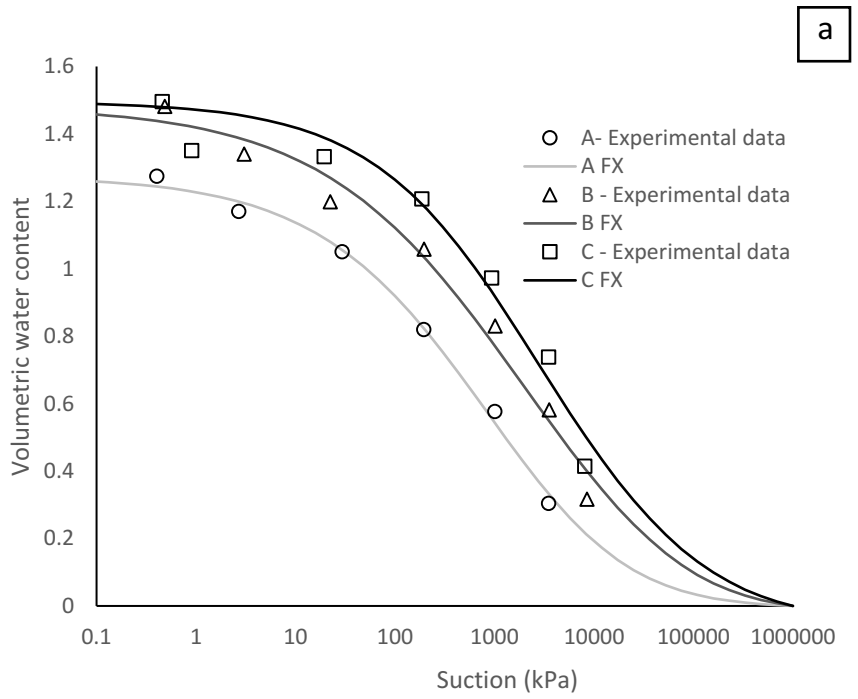
a
1.6
1.4
1.2
1
0.8
0.6
0.4
0.2
0
Volumetric water content
0.1
1
10
100
1000
10000
100000
1000000
Suction (kPa)
A- Experimental data
A FX
B - Experimental data
B FX
C - Experimental data
C FX

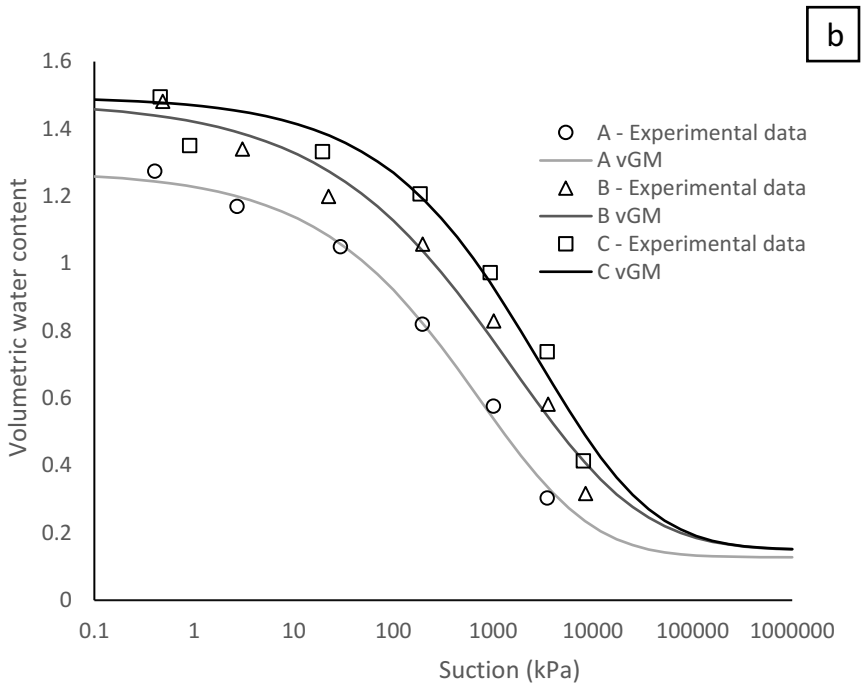
b
1.6
1.4
1.2
1
0.8
0.6
0.4
0.2
0
Volumetric water content
0.1
1
10
100
1000
10000
100000
1000000
Suction (kPa)
A - Experimental data
A vGM
B - Experimental data
B vGM
C - Experimental data
C vGM

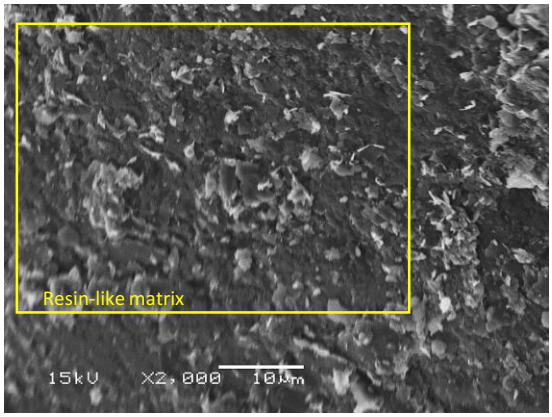
Resin-like matrix
15kV X2,000 10μm

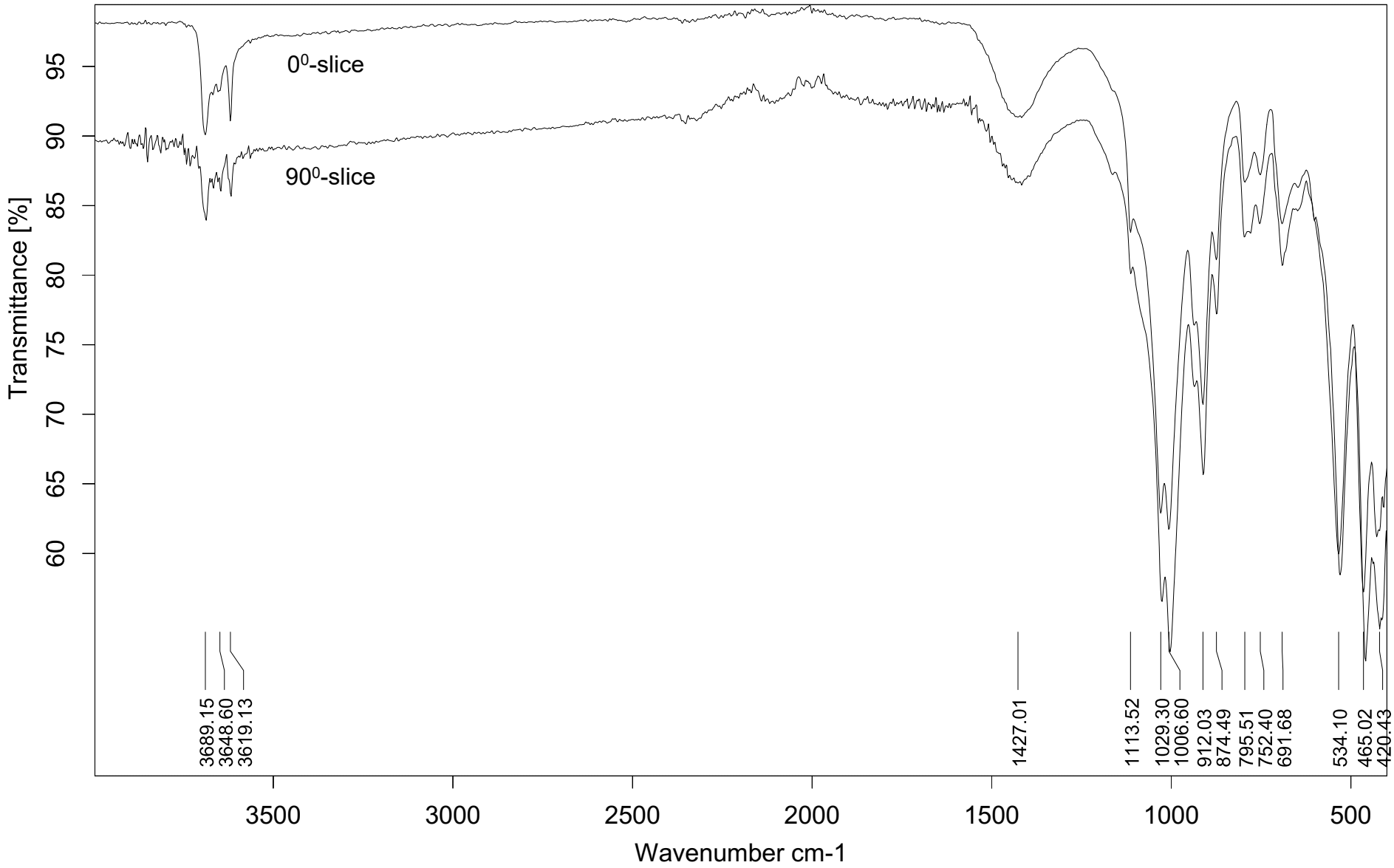
0⁰-slice
90⁰-slice
Transmittance [%]
95
90
85
80
75
70
65
60
3689.15
3648.60
3619.13
1427.01
1113.52
1029.30
1006.60
912.03
874.49
795.51
752.40
691.68
534.10
465.02
420.43
3500
3000
2500
2000
1500
1000
500
Wavenumber cm-1

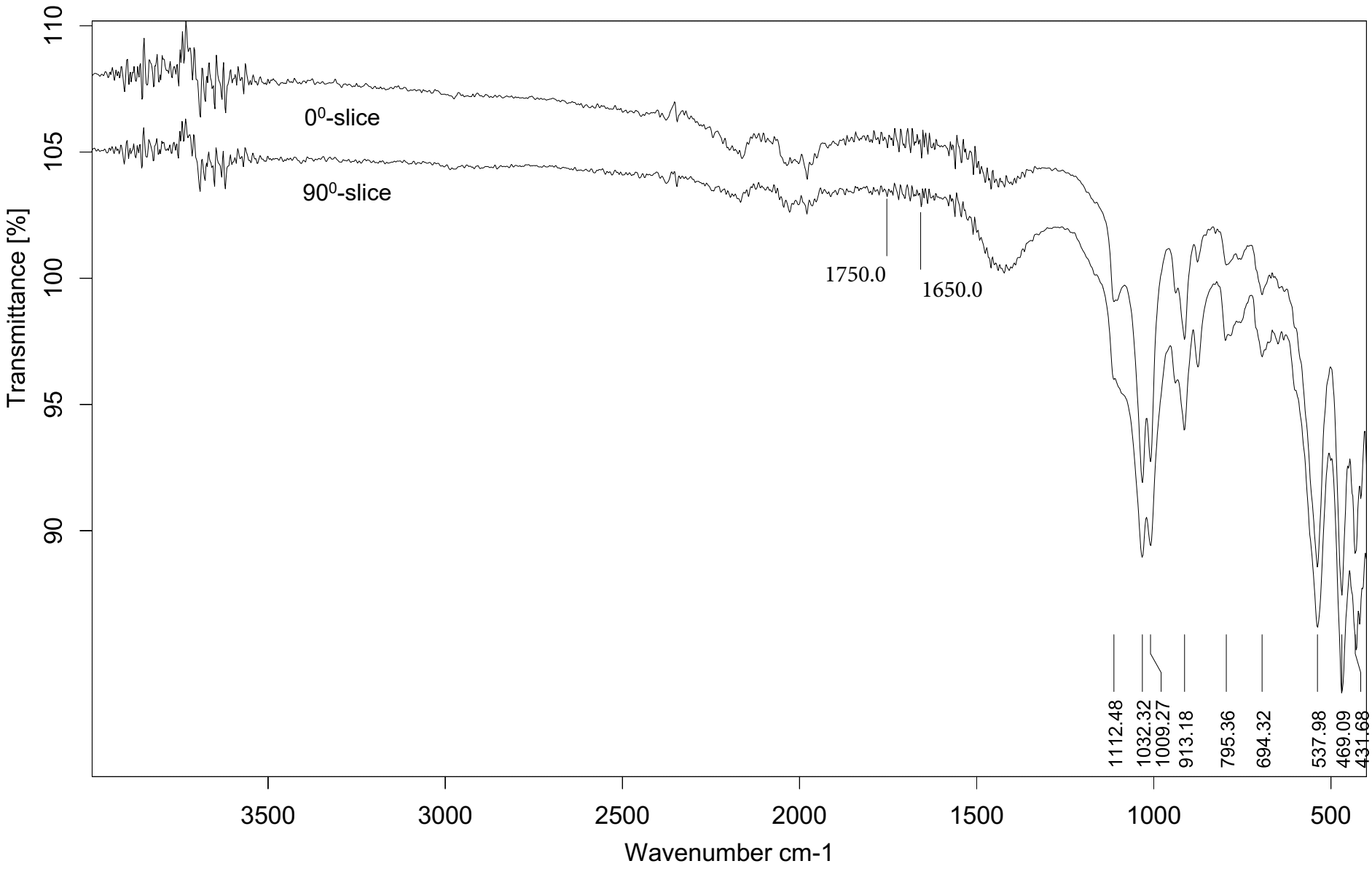
Transmittance [%]
110
105
100
95
90
0⁰-slice
90⁰-slice
1750.0
1650.0
1112.48
1032.32
1009.27
913.18
795.36
694.32
537.98
469.09
431.68
3500
3000
2500
2000
1500
1000
500
Wavenumber cm-1

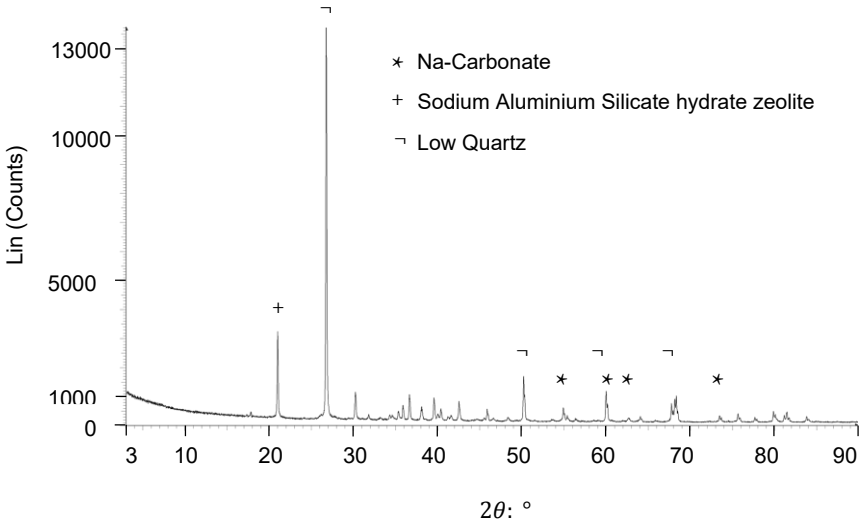
Na-Carbonate
Sodium Aluminium Silicate hydrate zeolite
Low Quartz
Lin (Counts)
13000
10000
5000
1000
0
3
10
20
30
40
50
60
70
80
90
2θ: °

$$\left[:\ddot{O}=Si\left|\begin{matrix}OH\\OH\end{matrix}\right.\right]^{\pm0}$$

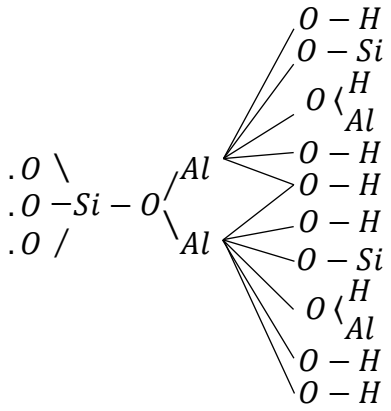

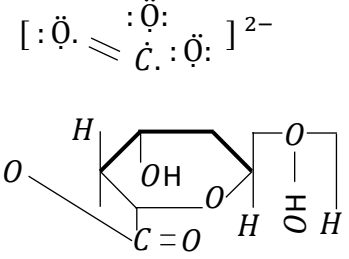

$$2Na. \quad .Cl \quad .Ca.$$

a

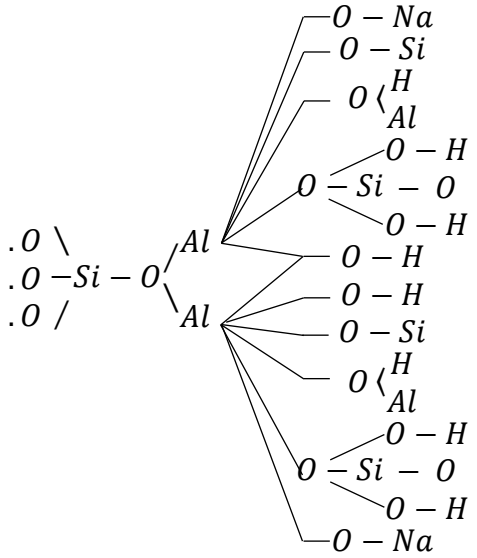
O − Na
O − Si
O
H
Al
O − H
O − Si − O
O − H
O − H
O − H
O − Si
O
H
Al
O − H
O − Si − O
O − H
O − Na
. O \
. O − Si − O
. O /
Al
Al

b

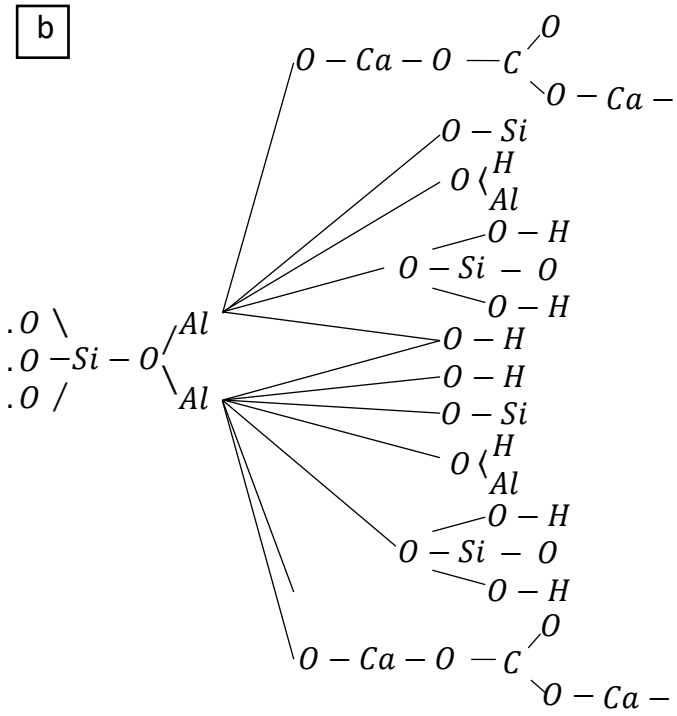
O − Ca − O — C
O
O − Ca −
O − Si
O
H
Al
O − H
O − Si − O
O − H
O − H
O − H
O − Si
O
H
Al
O − H
O − Si − O
O − H
O − Ca − O — C
O
O − Ca −
. O \
. O − Si − O
. O /
Al
Al

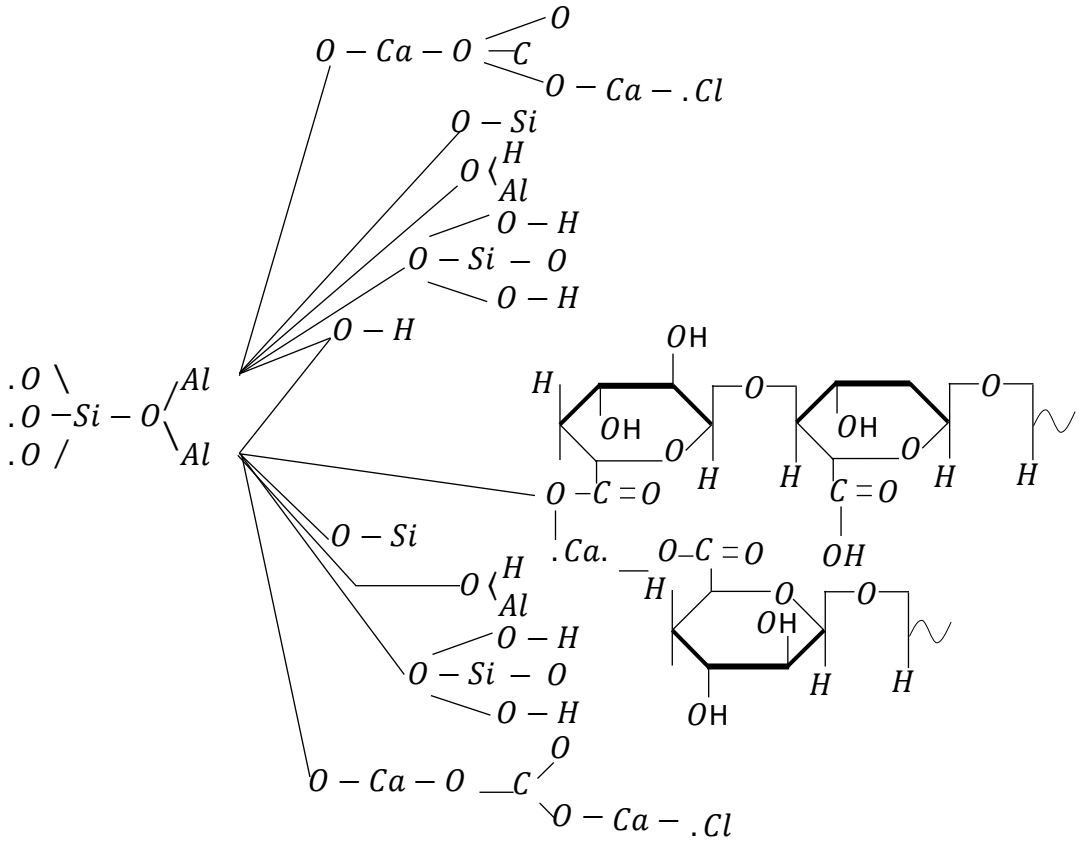

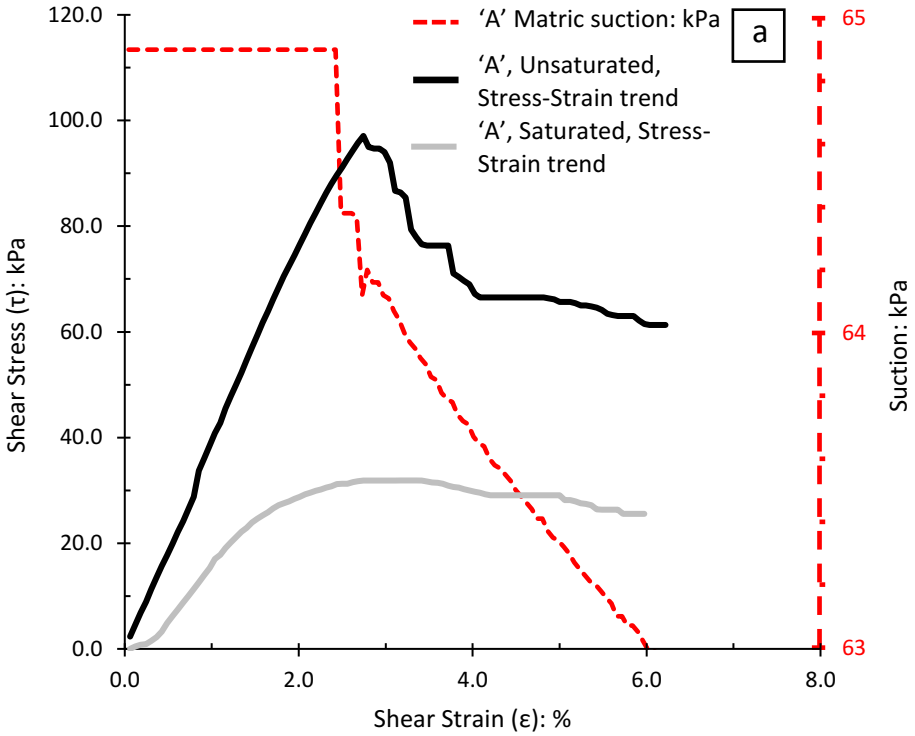
'A' Matric suction: kPa
'A', Unsaturated, Stress-Strain trend
'A', Saturated, Stress-Strain trend
a
120.0
100.0
80.0
60.0
40.0
20.0
0.0
Shear Stress (τ): kPa
0.0
2.0
4.0
6.0
8.0
Shear Strain (ε): %
65
64
63
Suction: kPa

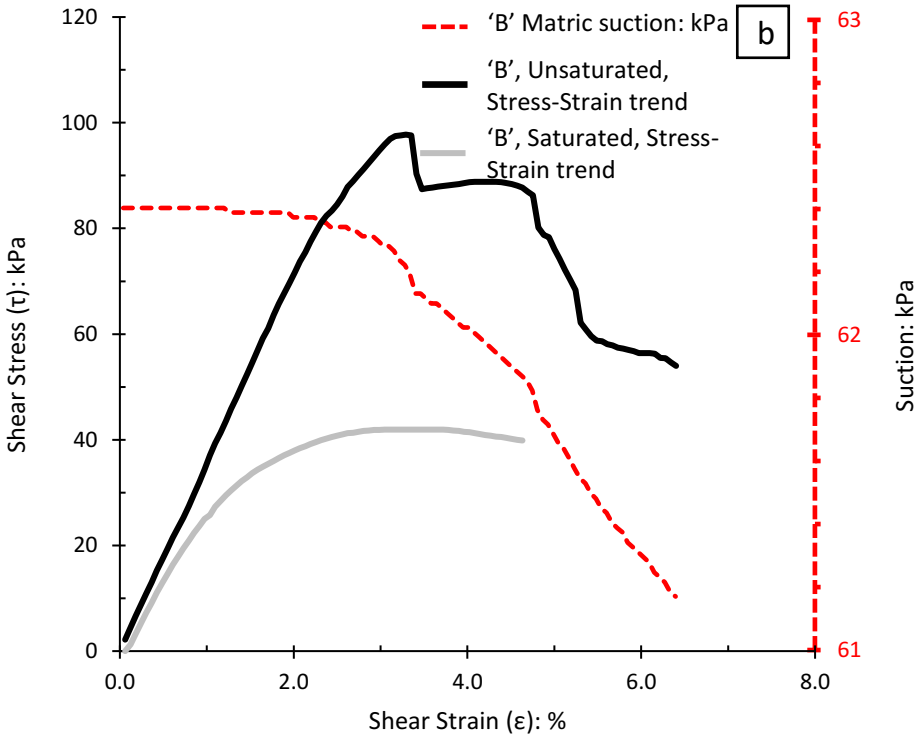
'B' Matric suction: kPa
'B', Unsaturated, Stress-Strain trend
'B', Saturated, Stress-Strain trend
b
Shear Stress (τ): kPa
Suction: kPa
Shear Strain (ε): %
120
100
80
60
40
20
0
63
62
61
0.0
2.0
4.0
6.0
8.0

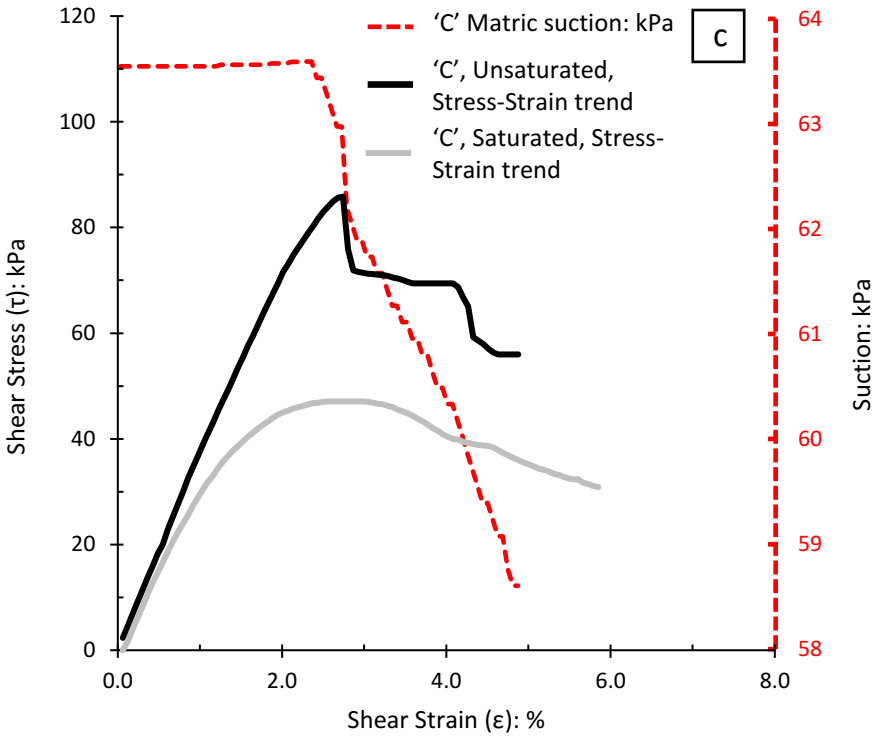
'C' Matric suction: kPa
'C', Unsaturated, Stress-Strain trend
'C', Saturated, Stress-Strain trend
C
Shear Stress (τ): kPa
Suction: kPa
Shear Strain (ε): %
120
100
80
60
40
20
0
64
63
62
61
60
59
58
0.0
2.0
4.0
6.0
8.0

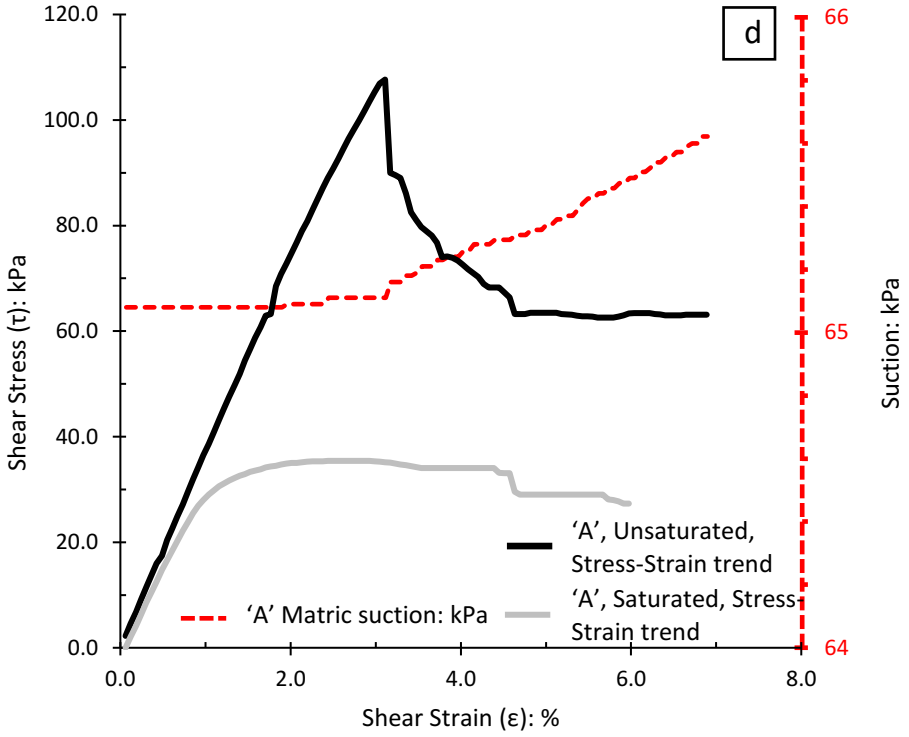
d
120.0
100.0
80.0
60.0
40.0
20.0
0.0
Shear Stress (τ): kPa
0.0
2.0
4.0
6.0
8.0
Shear Strain (ε): %
66
65
64
Suction: kPa
'A' Matric suction: kPa
'A', Unsaturated, Stress-Strain trend
'A', Saturated, Stress-Strain trend

.

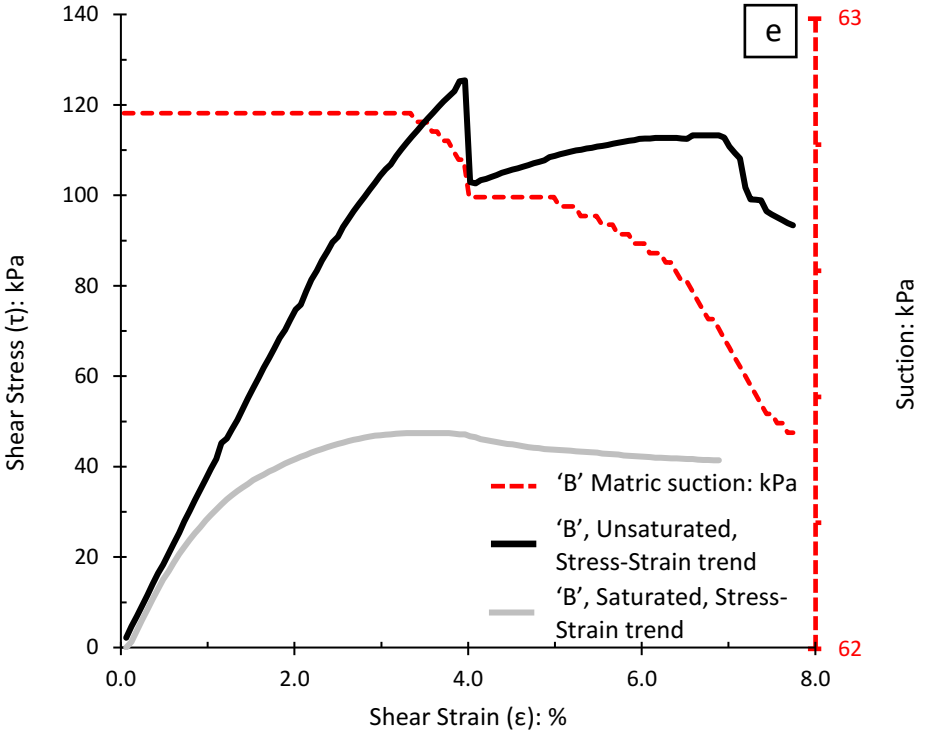
e
140
120
100
80
60
40
20
0
0.0
2.0
4.0
6.0
8.0
Shear Stress (τ): kPa
Shear Strain (ε): %
Suction: kPa
63
62
'B' Matric suction: kPa
'B', Unsaturated, Stress-Strain trend
'B', Saturated, Stress-Strain trend

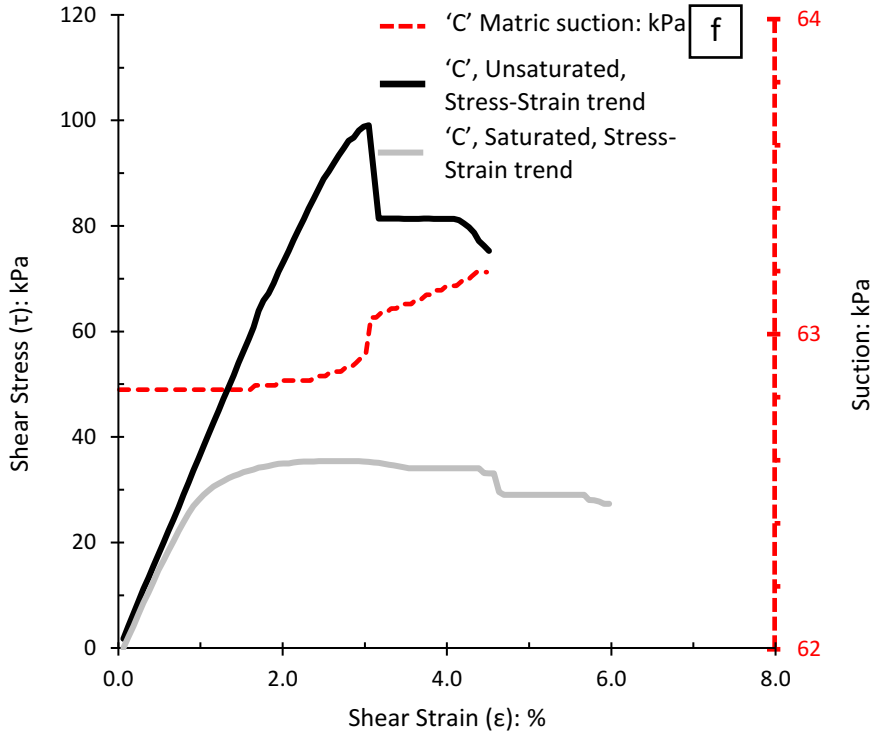
'C' Matric suction: kPa
f
'C', Unsaturated, Stress-Strain trend
'C', Saturated, Stress-Strain trend
Shear Stress (τ): kPa
Suction: kPa
Shear Strain (ε): %
120
100
80
60
40
20
0
64
63
62
0.0
2.0
4.0
6.0
8.0

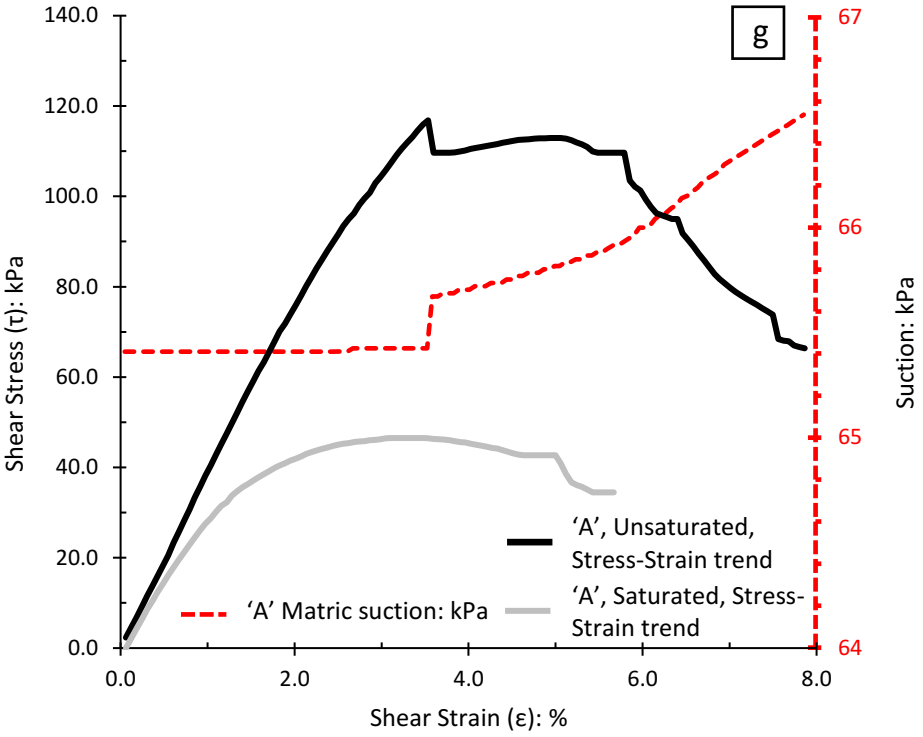
g
140.0
120.0
100.0
80.0
60.0
40.0
20.0
0.0
Shear Stress (τ): kPa
0.0
2.0
4.0
6.0
8.0
Shear Strain (ε): %
67
66
65
64
Suction: kPa
'A' Matric suction: kPa
'A', Unsaturated, Stress-Strain trend
'A', Saturated, Stress-Strain trend

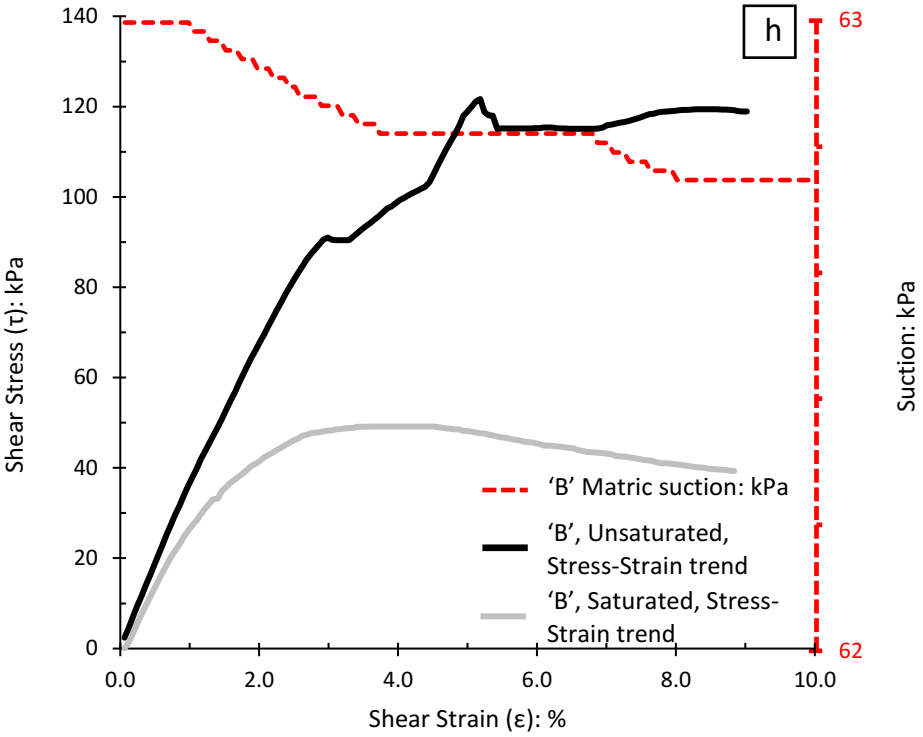
h
140
120
100
80
60
40
20
0
0.0
2.0
4.0
6.0
8.0
10.0
Shear Stress (τ): kPa
Shear Strain (ε): %
Suction: kPa
63
62
'B' Matric suction: kPa
'B', Unsaturated, Stress-Strain trend
'B', Saturated, Stress-Strain trend

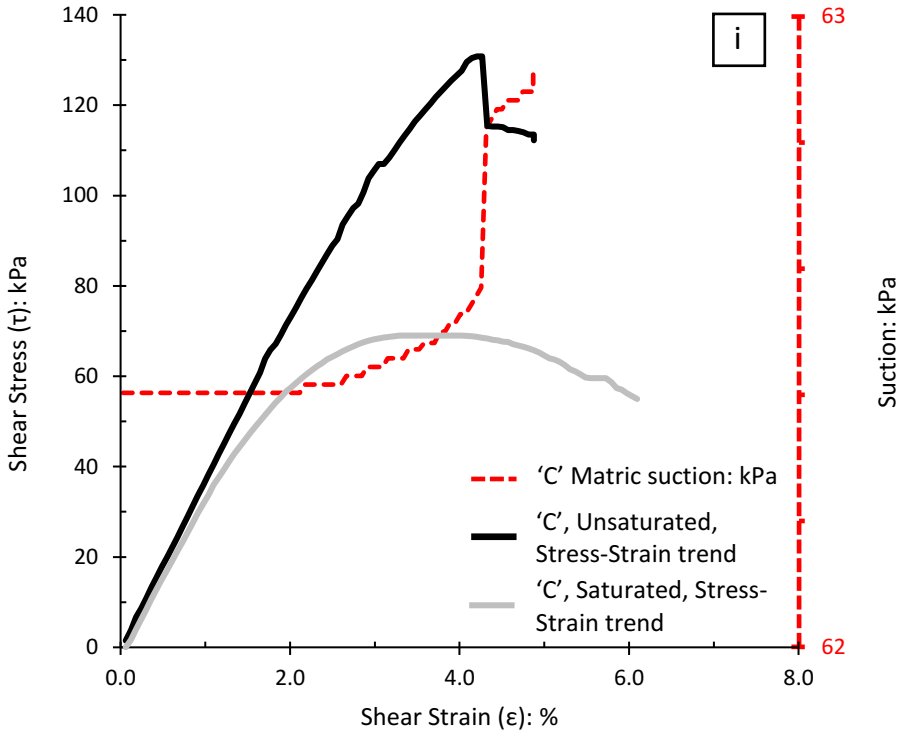
i
140
120
100
80
60
40
20
0
0.0
2.0
4.0
6.0
8.0
Shear Stress (τ): kPa
Shear Strain (ε): %
Suction: kPa
63
62
'C' Matric suction: kPa
'C', Unsaturated, Stress-Strain trend
'C', Saturated, Stress-Strain trend

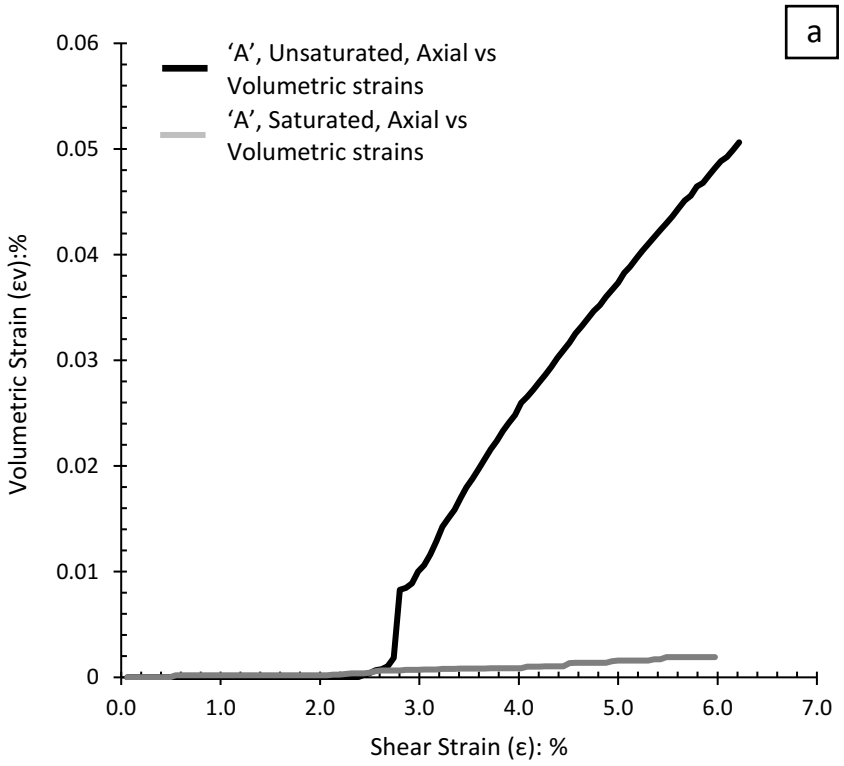
a
'A', Unsaturated, Axial vs Volumetric strains
'A', Saturated, Axial vs Volumetric strains
Volumetric Strain (εv):%
0.06
0.05
0.04
0.03
0.02
0.01
0
0.0
1.0
2.0
3.0
4.0
5.0
6.0
7.0
Shear Strain (ε): %

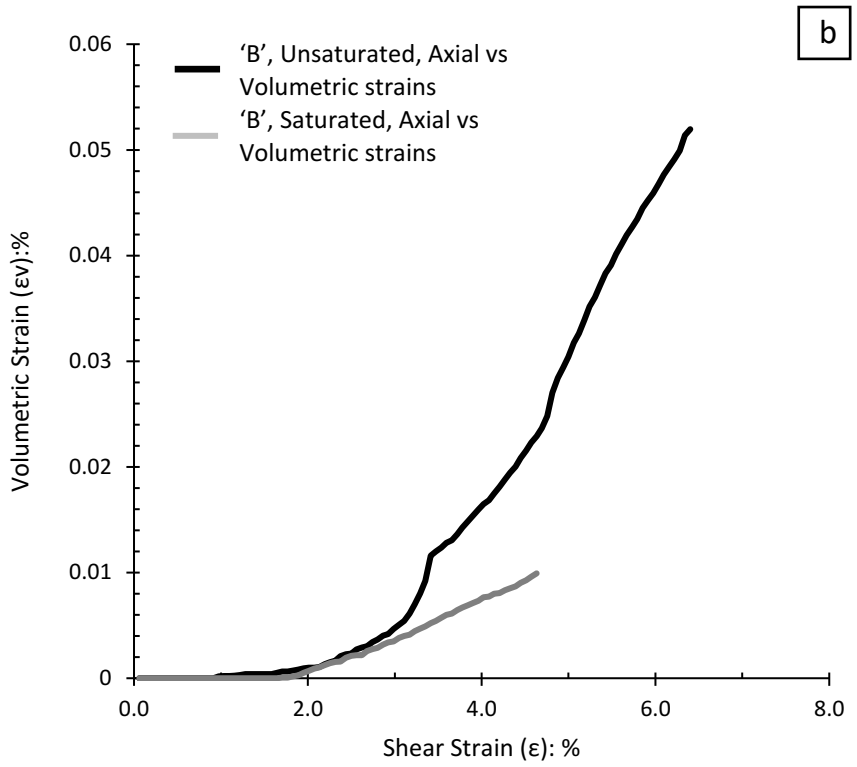
b
'B', Unsaturated, Axial vs Volumetric strains
'B', Saturated, Axial vs Volumetric strains
Volumetric Strain (εv):%
0.06
0.05
0.04
0.03
0.02
0.01
0
0.0
2.0
4.0
6.0
8.0
Shear Strain (ε): %

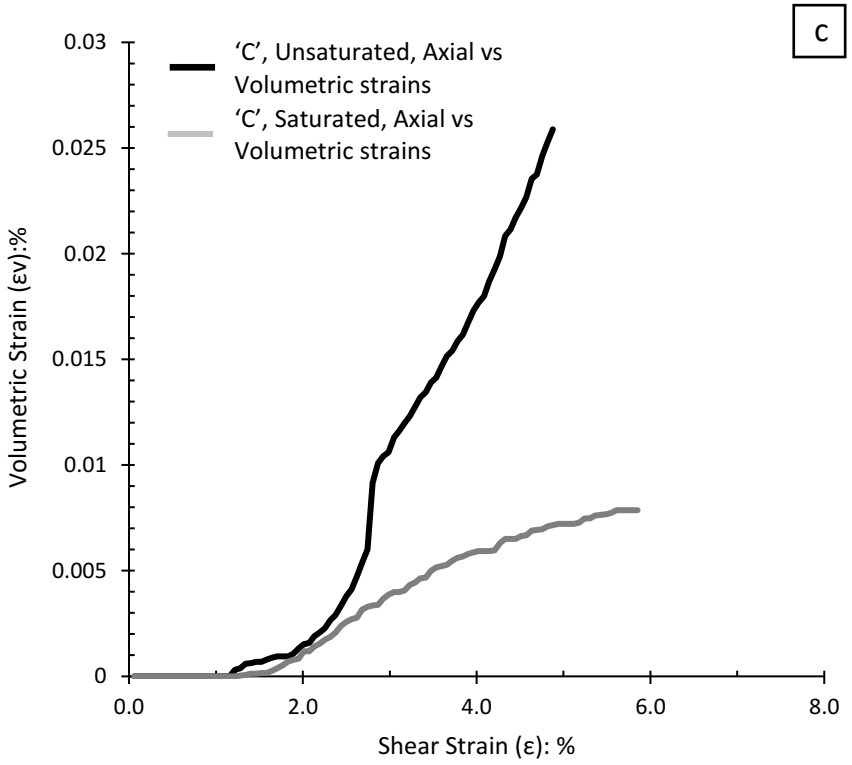
C
'C', Unsaturated, Axial vs Volumetric strains
'C', Saturated, Axial vs Volumetric strains
Volumetric Strain (εv):%
0.03
0.025
0.02
0.015
0.01
0.005
0
0.0
2.0
4.0
6.0
8.0
Shear Strain (ε): %

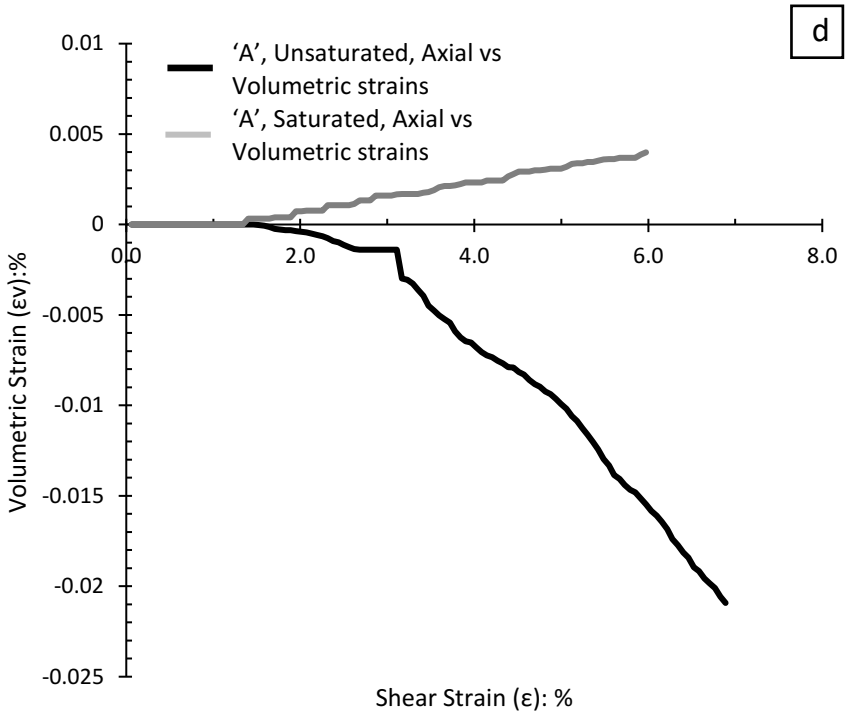
d
'A', Unsaturated, Axial vs Volumetric strains
'A', Saturated, Axial vs Volumetric strains
0.01
0.005
0
-0.005
-0.01
-0.015
-0.02
-0.025
0.0
2.0
4.0
6.0
8.0
Volumetric Strain (εv):%
Shear Strain (ε): %

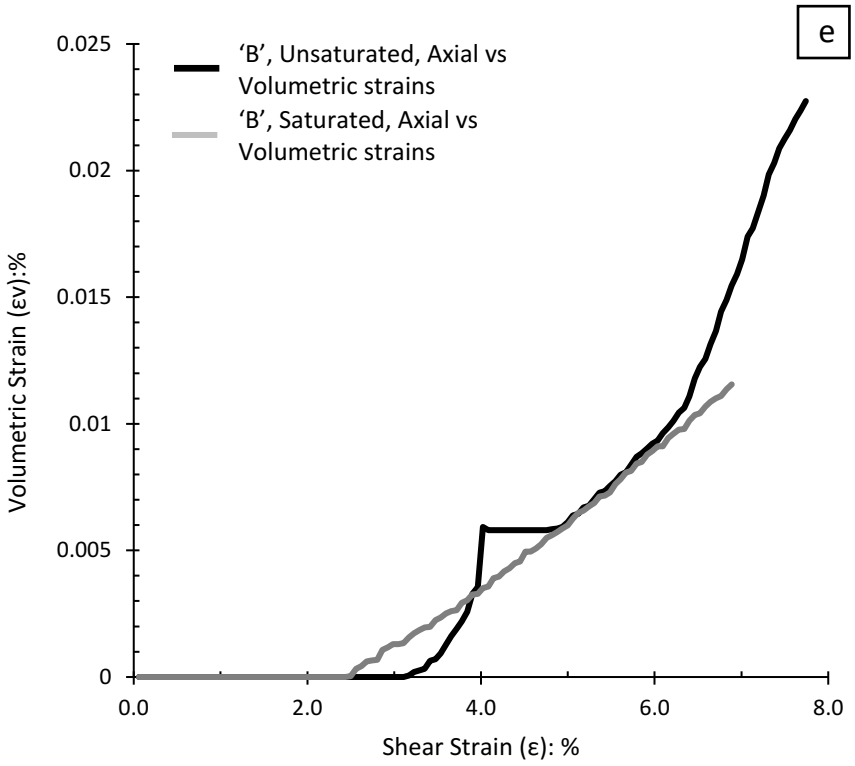
e
'B', Unsaturated, Axial vs Volumetric strains
'B', Saturated, Axial vs Volumetric strains
Volumetric Strain (εv):%
0.025
0.02
0.015
0.01
0.005
0
0.0
2.0
4.0
6.0
8.0
Shear Strain (ε): %

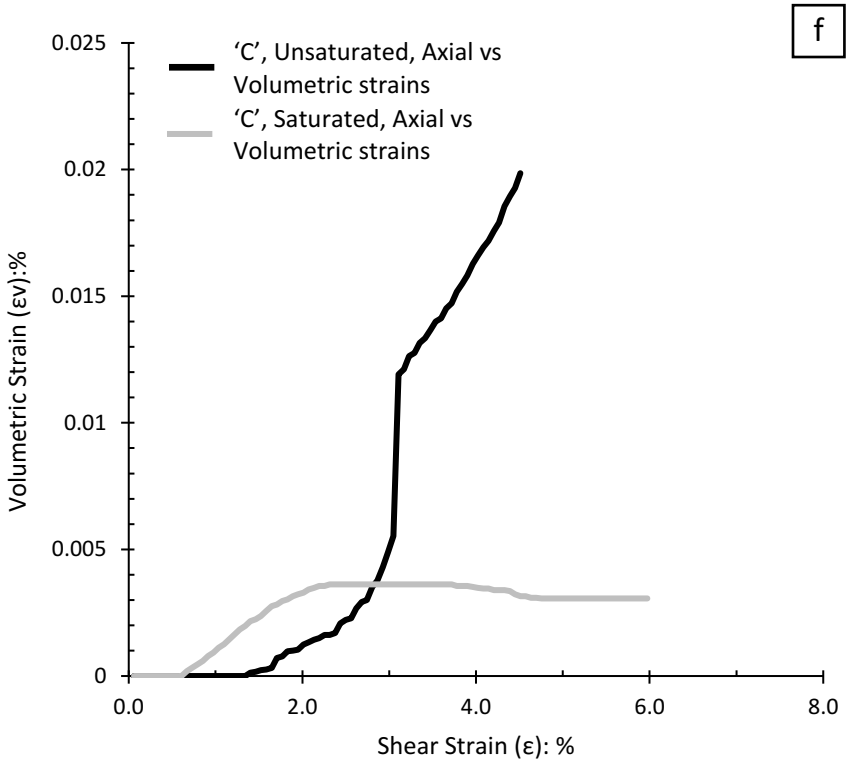
f
'C', Unsaturated, Axial vs Volumetric strains
'C', Saturated, Axial vs Volumetric strains
Volumetric Strain (εv):%
0.025
0.02
0.015
0.01
0.005
0
0.0
2.0
4.0
6.0
8.0
Shear Strain (ε): %

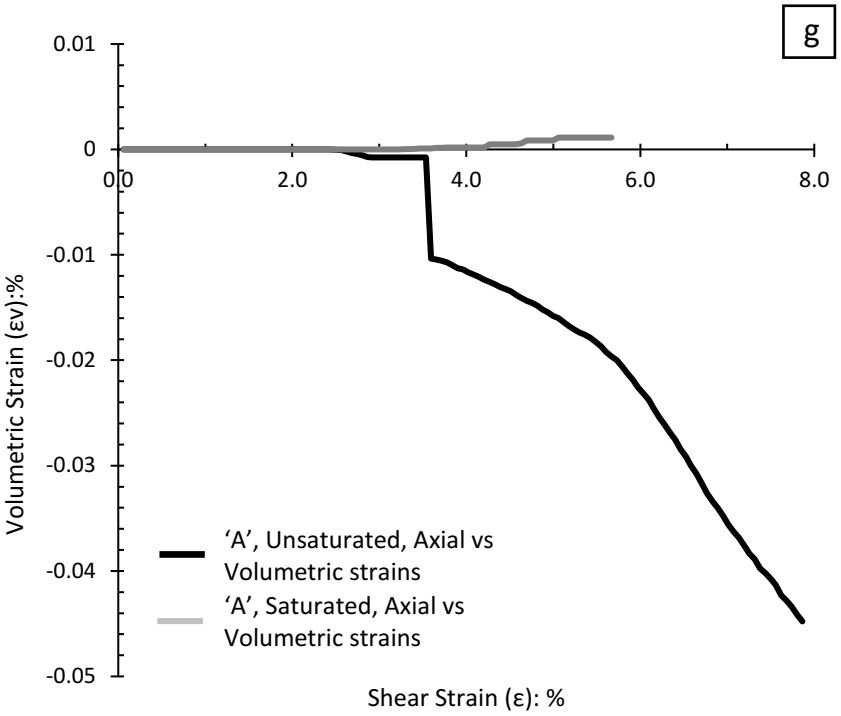
g
0.01
0
0.0
2.0
4.0
6.0
8.0
-0.01
-0.02
-0.03
-0.04
-0.05
Volumetric Strain (εv):%
'A', Unsaturated, Axial vs Volumetric strains
'A', Saturated, Axial vs Volumetric strains
Shear Strain (ε): %

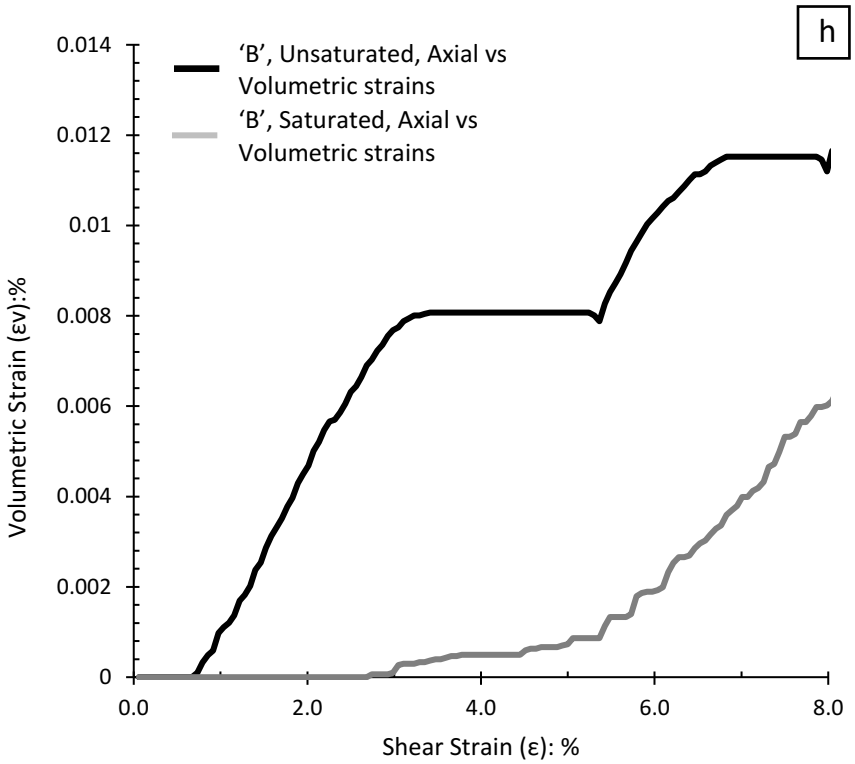
h
'B', Unsaturated, Axial vs Volumetric strains
'B', Saturated, Axial vs Volumetric strains
Volumetric Strain (εv):%
0.014
0.012
0.01
0.008
0.006
0.004
0.002
0
0.0
2.0
4.0
6.0
8.0
Shear Strain (ε): %

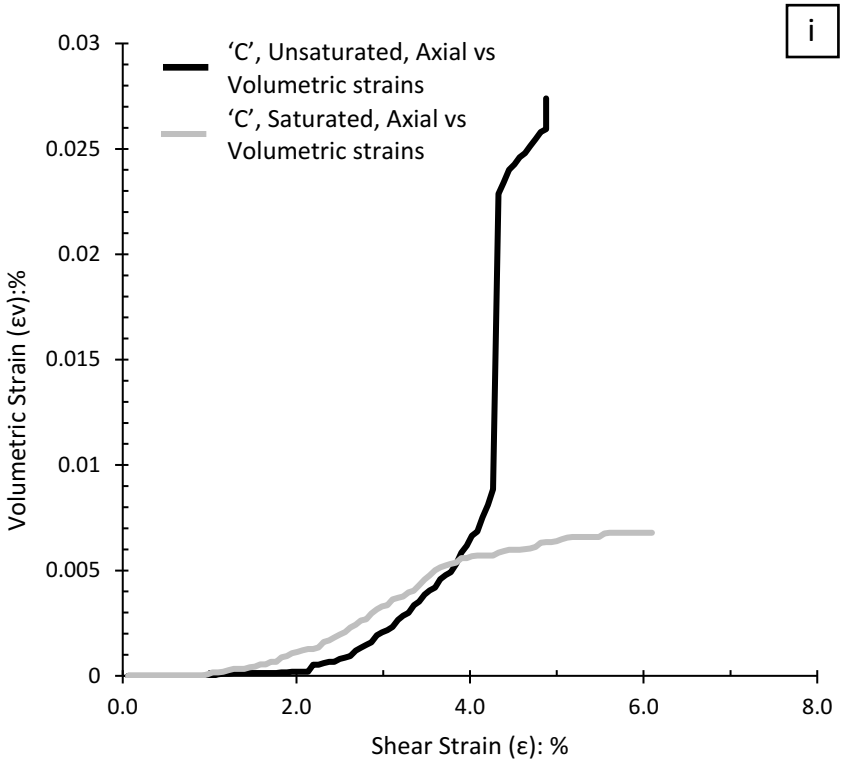
i
'C', Unsaturated, Axial vs Volumetric strains
'C', Saturated, Axial vs Volumetric strains
Volumetric Strain (εv):%
0.03
0.025
0.02
0.015
0.01
0.005
0
0.0
2.0
4.0
6.0
8.0
Shear Strain (ε): %